Physicochemical Characterization of Anionic Lipid Membranes under Low and High Ionic Strength: Effects of Moxifloxacin Assessed by Calorimetry, Spin-label, Steady-State and Time-Resolved Fluorescence

Journal:	*ACS Omega*
Manuscript ID	ao-2025-11663z
Manuscript Type:	Article
Date Submitted by the Author:	26-Nov-2025

Complete List of Authors:	Barrios Solano, Arthur; Universidade de São Paulo C. de Souza, Mariana; Universidade de São Paulo, Instituto de Física V. Medeiros, Carla; Universidade de Brasília, Instituto de Química S. Borges, Arthur; Universidade de Brasília Sugamosto, Bruno; Universidade de Brasília Duarte, Evandro; Universidade de Sao Paulo Instituto de Fisica, Physics Institute Lamy, Maria; Universidade de São Paulo Instituto de Física, Departamento de Física Geral Vignoli Muniz, Gabriel; Universidade de Brasilia,

Physicochemical Characterization of Anionic Lipid Membranes under Low and High Ionic Strength: Effects of Moxifloxacin Assessed by Calorimetry, Spin-label, Steady-State and Time-Resolved Fluorescence

Arthur Henrique Barrios Solano[b], Mariana C. Souza[b], Carla C. V. Medeiros[a], Arthur S. Borges[a], Bruno Sugamosto[a], Evandro L. Duarte[b], M. Teresa Lamy[b], and Gabriel S. Vignoli Muniz[a,b]

[a]Instituto de Química, Universidade de Brasília, CEP 70910-900, Campus Universitário Darcy Ribeiro, Brasília, Brasil

[b]Instituto de Física, Universidade de São Paulo, CEP 05508-090, Cidade Universitária, São Paulo, Brasil

[*]Corresponding authors: Gabriel S. Vignoli Muniz (gabriel.vignoli@unb.br)

Abstract

In the present study, we comparatively investigate the interaction between the antibiotic moxifloxacin (MFX) and extruded (100 nm) lipid vesicles composed of the anionic lipid 1,2-dipalmitoyl-sn-glycero-3-phospho-(1'-rac-glycerol) (DPPG), under both low ([NaCl] = 3 mmol L^{-1}) and high ionic strength conditions ([NaCl] = 150 mmol L^{-1}). By employing differential scanning calorimetry (DSC) and electron spin resonance (ESR) spectroscopy with spin-labeled lipids positioned at two distinct depths within the bilayer, we evaluated structural alterations induced by increasing concentrations of MFX. Additionally, taking advantage of the intrinsic fluorescence of the antibiotic, we monitored structural changes and determined its affinity for the anionic bilayers upon exposure to rising concentrations of liposomes under different configurations: gel and fluid phases.

MFX was found to induce a narrowing of the main gel-to-fluid phase transition peak of DPPG under both ionic strengths, indicating enhanced cooperativity of the thermal lipid transition. ESR spectra of spin labels inserted at the 5th carbon position, near the interfacial region between the polar headgroups and the hydrophobic core, and deeper within the bilayer revealed that MFX promotes tighter lipid packing and decreases the local polarity of the membrane interior, independently of salt concentration.

Upon increasing the concentration of anionic liposomes, the MFX emission displays a relative redshift. The data suggest that, upon interaction with the anionic bilayers, a fraction of the zwitterionic MFX molecules undergoes protonation, presumably driven by a locally low pH microenvironment at the vesicle interface.

MFX fluorescence lifetimes are enhanced by its association with gel and fluid liposomes, enabling the determination of membrane–water partition coefficients, which were found to be $K_p = (2.5 \pm 0.2) \times 10^4$ and $(1.4 \pm 0.1) \times 10^4$ for the gel and fluid phases, respectively, under low ionic strength conditions. Furthermore, given the relevance of antibiotic–membrane interactions to antimicrobial efficacy, toxicity, and drug delivery strategies, the findings reported herein advance the understanding of the physicochemical behavior of MFX in lipid environments and may guide the rational development of membrane-targeting antibiotics and lipid-based delivery systems.

Keywords: Structural characterization; DPPG; Moxifloxacin; Steady-state and time-resolved fluorescence; DSC; Spin Label ESR.

1. Introduction

Fluoroquinolones (FQs) are a widely used class of antibiotics in both human and veterinary medicine. Their well-established mechanism of action involves the inhibition of the bacterial enzymes topoisomerase II and IV, through the formation of stable drug–enzyme–DNA complexes [1]. Consequently, FQs must reach the bacterial cytosol to exert their antimicrobial effects. To penetrate the cytosol of Gram-negative bacteria, many fluoroquinolones rely on porin channels to cross the outer membrane. [1,2]. Particularly, 1-Cyclopropyl-7-(2,8-diazabicyclo[4.3.0]non-8-yl)-6-fluoro-8-methoxy-4-oxoquinoline-3-carboxylic acid, better known as moxifloxacin (MFX; Fig.1), is a potent FQ with activity against both Gram-positive and Gram-negative bacteria. Regarding its uptake in Gram-negative bacteria, MFX appears to have little dependence on porin channels, suggesting that interactions between this antibiotic and membrane lipids may play an important role in facilitating its access to the cytosol [3,4].

Studies with MFX and model membranes have shown that the antibiotic interacts with lipids. High concentrations of MFX induce dramatic structural alterations in extruded lipid dispersions composed of pure 1,2-dipalmitoyl-sn-glycero-3-phosphocholine (DPPC) and DPPC:cardiolipin (CL) mixtures (8:2 molar ratio), using a lipid-to-antibiotic molar ratio of approximately 1:1 [5]. Also, the interaction between MFX and zwitterionic membranes composed of 1,2-dimyristoyl-sn-glycero-3-phosphocholine (DMPC) or 1,2-dimyristoyl-sn-glycero-3-phosphorylglycerol (DMPG), was investigated showing that MFX has much higher affinity for anionic liposomes, and fluorescence probes and spin labels embedded into lipid bilayers strongly indicates that MFX acts in the surface of anionic DMPG vesicles [6].

Phosphatidylglycerol (PG) is the most abundant anionic lipid in bacterial membranes [7]. As such, it has become a frequent target in the development of antimicrobial drugs [7,8]. Moreover, the interaction of drugs with anionic lipids may plays a key role in their ability to penetrate bacterial membranes and reach the cytosol, as observed in the case of moxifloxacin (MFX) [4]. PG lipids have also been explored in the formulation of drug delivery systems due to their biocompatibility and functional properties [9].

To better understand the interaction between MFX and anionic lipids, and to provide insights that may aid in the design of more effective drug delivery systems, we investigated the interaction of MFX with 1,2-dipalmitoylphosphatidylglycerol (DPPG) liposomes. We employed two distinct liposome configurations: one in the gel phase, representing more ordered and tightly packed membrane regions, and another in the fluid phase, mimicking more disordered and dynamic areas of bacterial membranes. As an initial step, we focused on liposomes composed of a single lipid component to reduce complexity and generate a solid basis for interpreting interactions in more complex lipid systems in future studies.

In this work, we monitored liposome structural properties using differential scanning calorimetry (DSC) and electron spin resonance (ESR) with spin probes inserted at different depths of the bilayers. The antibiotic's behavior and environment were assessed via its intrinsic fluorescence, using both steady-state and time-resolved fluorescence spectroscopy. Considering that liposome structure and drug-lipid interactions are influenced by ionic strength [10,11], all experiments were performed under both low ionic strength ([NaCl] = 3 mmol L^{-1}) and physiological ionic strength conditions ([NaCl] = 150 mmol L^{-1}).

Thus, this work contributes to a deeper understanding of how antibiotics relate to lipid assemblies, providing information that may support the development of more efficient and

targeted drug-delivery systems, while also offering a clearer view of the mechanisms governing the action and cellular uptake of moxifloxacin across bacterial membranes.

2.Materials & methods

2.1. Chemical and Reagents

Sodium salt of 1,2-dipalmitoyl-*sn*-glycero-3-phospho-(1'-rac-glycerol) (DPPG), spin labels 1-palmitoyl-2-(*n*-doxylstearoyl)-*sn*-glycero-3-phosphocholine (*n*-PCSL, *n*= 5 or 16) were acquired from Avanti Polar Lipids. Moxifloxacin (MFX), 4-(2-hydroxyethyl)-1-piperazineethanesulfonic acid (HEPES), ethylenediaminetetraacetic acid (EDTA), boric acid, phosphoric acid 85%, citric acid, sodium hydroxide (NaOH), hydrochloric acid (HCl), chloroform, methanol, and sodium chloride (NaCl) were purchased from Merck (St Louis, MO). All solutions or dispersions were prepared using Milli-Q water or a mixture of chloroform and methanol.

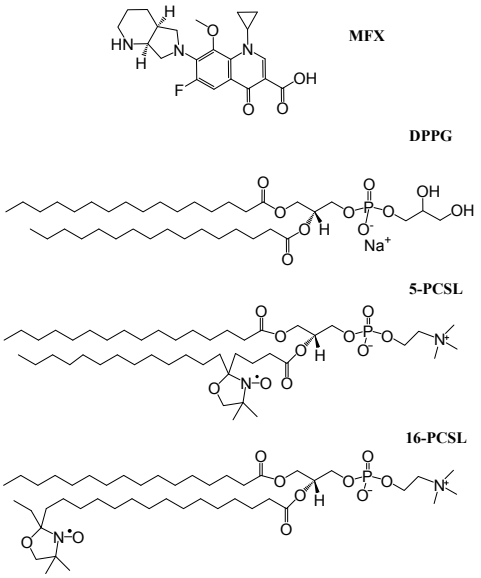

Figure 1. At the top, schematic chemical structure of the antibiotic moxifloxacin. At the bottom, the chemical structures of the anionic lipid DPPG, and the paramagnetic probes 5-PCSL and 16-PCSL.

2.2 Sample preparations

Lipids were dissolved in a mixture of chloroform and methanol (6:1). For ESR experiments, spin labels 5-PCSL (0.8 mol%) or 16-PCSL (0.3 mol%) were added to the lipid solution in which the percentage referred to the final lipid concentration. Then, the solution was dried under a stream of ultra-pure nitrogen gas, thus a thin film of lipids was formed at the bottom of the glass tube. The lipid film was kept under low pressure conditions for a minimum of three hours to eliminate any trace of organic solvent. Lipid dispersions were prepared by the addition of buffer to the lipid film and subjecting it to intense vortexing for 2 minutes at 60°C, repeated four times. Finally, lipid dispersions were extruded through polycarbonate filters (mini-extruder by Avanti Polar Lipids, 19 mm membranes with 100 nm pores, 31 times) above the lipid gel−fluid transition temperature (≥ 60ºC) to form large unilamellar vesicles (LUVs). All lipid dispersions used in this work were freshly prepared on the day the experiments were conducted. The buffers used in this study consisted of 10 mmol L^{-1} HEPES, 1 mmol L^{-1} EDTA, pH 7.4, with either 3 mmol L^{-1} NaCl (low ionic strength) or 150 mmol L^{-1} NaCl (high ionic strength). For the determination of MFX pKa values, a universal buffer was used, composed of a mixture of 33 mmol L^{-1} citric acid, 50 mmol L^{-1} phosphoric acid, 50 mmol L^{-1} boric acid, and 330 mmol L^{-1} NaOH in its stock solution. The universal buffer was prepared by diluting the stock buffer at a ratio of 1:15 in water and adjusting the pH using a 1 mol L^{-1} HCl solution [12].

MFX was dissolved in methanol (6 mmol L^{-1}). A desired amount of this solution was placed in a glass tube and dried under a stream of ultra-pure nitrogen gas, thus obtaining an antibiotic film at the bottom of the glass tube. To eliminate any organic solvent trace, MFX films were submitted to low pressure conditions for at least 3 hours. Finally, MFX films were

hydrated with buffer or LUV dispersions followed by an intense vortexing for 2 minutes at 60 ºC, four times. Finally, the samples were incubated for 30 minutes at room temperature before the measurements.

2.3 Differential Scanning Calorimetry (DSC)

DSC thermograms were obtained with a microcalorimeter (Microcal VP-DSC, Northampton, MA). Each sample was scanned five times. The first scan was performed at a rate of 90ºC per hour and used as an annealing step to eliminate the sample's thermal history, and was not included in the data analysis. The next four scans, two endothermic and two exothermic, were runed at the rate of 20ºC per hour, with temperatures ranging from 15ºC to 60ºC. The scans were found to be reproductible. The sample cell (500 μL) was filled with a 3 mmol L^{-1} lipid dispersion with or without the desired concentration of MFX, as described in *2.2*. In this work, we often refer to the concentration of MFX as the percentage of the antibiotic with respect to the molar concentration of the lipid (mol % [MFX] = 100 [MFX]/[L]), where [MFX] and [L] are MFX and lipid molar concentrations, respectively. By using MicroCal Origin software, with the additional module for DSC data analysis provided by MicroCal, we determined thermodynamic parameters such as the enthalpy variation (ΔH), the position of the maximum of the gel-fluid temperature transition peak, T_m, and the width at half maximum ($\Delta T_{1/2}$).

2.4 Electron spin resonance (ESR) spectroscopy

X-band electron spin resonance spectra were obtained with a Bruker EMX spectrometer. Field modulation amplitude of 1 or 2 G and microwave power of 13 mW were

used. The temperature ranged from 10 ºC to 60 ºC, controlled by a Bruker BVY-2000 variable temperature device. ESR data were analyzed using the software WINEPR.

The maximum ($2\,A_{max}$), and inner ($2\,A_{min}$) hyperfine splittings were measured directly on the 5-PCSL ESR spectra, and, for fluid membranes, the effective order parameter (S_{eff}) and the isotropic hyperfine splitting (a_0) were calculated according to equations 1:

$$S_{eff} = \frac{A_{\parallel} - A_{\perp}}{A_{zz} - (1/2)(A_{xx} + A_{yy})} \frac{a'_o}{a_o} \qquad \textbf{Eq. 1}$$

where

$$A_{||} \approx A_{max}$$

$$A_{\perp} = A_{min} + 1.4\,[1 - \frac{A_{\parallel} - A_{min}}{A_{zz} - (1/2)(A_{xx} + A_{yy})}$$

$$a'_0 = {}^{1}/_{3}\,(A_{zz} + A_{yy} + A_{xx})$$

$$a_0 = {}^{1}/_{3}\,(A_{||} + 2A_{\perp})$$

A_{zz}, A_{xx}, and A_{yy} are the principal values of the hyperfine tensor for 2-doxyl propane, 32.9, 5.9, and 5.4 Gauss, respectively [13,14]. With the spin label 16-PCSL, for gel liposomes, the central line width (ΔH_0) was directly measured on the 16-PCSL ESR spectra. At the fluid phase, the amplitude of the three hyperfine lines (h_{+1}, h_0, and h_{-1}) and isotropic hyperfine splitting (a_0) were also measured directly on the ESR 16-PCSL spectra. For more details, see Ref. [15]. The lipid concentration used was 3 mmol L^{-1}, with and without the desired MFX concentrations.

2.6 Ultraviolet-visible (UV-vis) absorption spectroscopy

Optical absorption spectra were obtained with an UV−vis spectrophotometer (Varian Cary 50, Santa Clara, CA). In all optical experiments, samples were placed in a quartz cuvette (0.2 × 1.0 cm, 400 µl), with the absorption optical pathway of 0.2 cm. The temperature was controlled with a Carry Peltier thermostat.

Samples were prepared according to the following protocol. MFX films (see Section *2.2*) were hydrated with ~~a~~ buffer solution to prepare a MFX stock solutions at 0.5 mmol L^{-1}. The stock was then, diluted using the same buffer and/or concentrated LUV dispersions (10 mmol L^{-1}, see Section *2.2*) to achieve a final MFX concentration of 8 µmol L^{-1}, with and without the desired liposome concentration. Next, the samples were quickly vortexed and left to equilibrate at room temperature for 5 minutes. Then, the samples were placed in the spectrometer previously set-up at 25 ºC, corresponding to the gel phase of DPPG bilayers. Then, to assure the thermal equilibrium, the sample was left for 5 minutes inside the spectrometer. The optical experiments were conducted in sequence, first the absorption spectra were registered, then the steady-state fluorescence spectra, and finally the fluorescence decay were measured. All the instruments were set at 25 ºC, as previously performed in our works [16–18]. Then, the temperature was increased to 50 ºC, corresponding to the fluid phase of dipalmitoyl bilayers, and the same protocol was followed.

2.7 Stead-state fluorescence spectroscopy

Steady-state fluorescence measurements were performed with a fluorimeter (Varian Cary Eclipse, Santa Clara, CA) with temperatures controlled by a Carry Peltier thermostat. Fluorescence experiments were performed using 400 µl solutions of 8 µmol L^{-1} MFX in buffer without or with LUVs, as described above. The experiments were conducted with an excitation beam light at 345 nm, with an optical pathway of 0.2 cm, with slits for excitation

and for emission of 5 nm. The inner filter correction [19] was applied to all the fluorescent emission spectra by using the following equation 2:

$$F_{corr}(\lambda) = F_{obs}(\lambda)10^{(A_{exc}\, l + A_{ems}(\lambda) l')} \qquad \textbf{Eq. 2}$$

where $F_{corr}(\lambda)$ and $F_{obs}(\lambda)$ are the corrected and observed fluorescence intensities, A_{exc} and $A_{ems}(\lambda)$ are the absorbance per unit of pathway at the excitation and emission wavelengths, respectively. l and l′ are the optical pathway in cm for excitation (0.1 cm), and for emission (0.5 cm), respectively, considering the cuvette centre.

2.8 Time resolved fluorescence spectroscopy

Time-resolved (TR) fluorescence measurements were performed using time-correlated single photon counting technique (TCSPC). The excitation light beam comes from a titanium-sapphire Tsunami 3950 laser from Spectra Physics (Newport Corporation, Irvine, CA, USA), pumped by a solid-state laser Millenia Pro model J80 also from Spectra Physics. The frequency of pulse picker (Spectra Physics model 3980-25) was 8 MHz. The Tsunami was set to give an output of 852 nm and a third harmonic generator BBO crystal (GWN-23PL Spectra Physics) was used to generate the excitation light at 284 nm. Although this is different from the excitation wavelength used in the steady state fluorescence experiments, 345 nm, it also corresponds to an absorption band of MFX. The MFX relaxation does not depend on the excitation wavelength Fig. **SM1**. At 284 nm, for time-resolved experiments, the signal-to-noise was much better than at 345 nm.

By using FAST software supplied by Edinburgh Photonics the data were fitted by applying the model of exponential decays [20] using the following equation 3:

$$F(\lambda,t) = \sum_{i=1}^{N} \alpha_i e^{-t/\tau_i} \qquad \textbf{Eq. 3}$$

where F(λ,t) is the number of photons emitted at a given wavelength (λ) and time, t is the time after the excitatory light beam, α_i is the pre-exponential factor, τ_i is the lifetime of the i^{th} component of the decay, and f_i is the fraction contribution of the lifetime τ_I to the intensity decay. All the fluorescence decay curves were well fitted by a biexponential model, as indicated by the reduced chi-square (χ^2) statistical parameter, $0.80 \leq \chi^2 \leq 1.33$, and resulting in two fluorescence lifetimes a short lifetime (τ_1) and a longer lifetime (τ_2)

The apparent partition constant (K_p) was obtained through non-linear fitting using a conventional isotherm [21], according to Eq. 4.

$$K_p \equiv \frac{n_L/V_L}{n_{aq}/V_{aq}} \qquad \textbf{Eq. 4}$$

$$\tau_2 = \frac{\tau_{2w} + K_p \gamma_L [L] \tau_{2L}}{1 + K_p \gamma_L [L]}$$

where n_L and n_{aq} are the number of moles of MFX in the membrane and aqueous phases, respectively. V_{aq} is the volume of the aqueous phase which is in a good approximation equal to the total volume (V_{total}.), taking into consideration both phases, aqueous and lipid. V_L is the volume of the lipid phase, $V_L = \gamma_L$ [L] V_{total}, γ_L is the molar volume of DPPG lipids. The values of γL were taken from literature data, yielding 0.67 L mol^{-1} for gel-phase DPPG membranes and 0.71 L mol^{-1} for fluid-phase membranes [22]. τ_2, τ_{2w}, and τ_{2L} correspond to

the longer fluorescence lifetime of MFX at a given lipid concentration, in the absence of lipids, and under lipid-saturation conditions, respectively [23].

2.9 Reproducibility and sample stability

Each experiment was performed in triplicate. The values display in this work consist of an average of the measurements and error values account for standard deviations and are presented as error bars when larger than the symbols. No vesicle precipitation was observed during the experiments. The samples were always visually checked before and after the measurements were taken. For optical absorption and fluorescence measurements, MFX spectra were quite reproducible after a minimum of 3 hours in the cuvette.

3.Results

3.1 Liposome modifications caused by moxifloxacin

Liposomes, commonly composed of a single saturated lipid species, often exhibit two distinct thermal phases: a gel phase and a fluid phase. In both phases, the lipids are arranged within the two-dimensional plane of the bilayer. However, lipid mobility differs significantly between these phases. In the gel phase, lipids are organized in a manner that displays lateral and crystalline order [24]. Conversely, in the fluid phase, lipids lack this order and exhibit greater movement along the axis of the paraffinic chains, displaying a more isotropic motion [24].

Exogenous molecules can interact differently with gel-phase and fluid-phase liposomes. To investigate this, we examined the interactions between MFX and DPPG bilayers in their gel and fluid phases, mimicking lipid domains with tighter packing and greater fluidity,

respectively, as observed in biological membranes. The structure and dynamics of acidic lipids, as well as their interactions with foreign molecules, are often influenced by ionic strength conditions [25,26]. Thus, we analyzed the interaction between the antibiotic and DPPG dispersions under low ([NaCl] = 3 mmol L^{-1}) and high ([NaCl] = 150 mmol L^{-1}) ionic strength conditions.

3.1.1 Differential scanning calorimetry (DSC)

The lipid gel-fluid phase transition is a phenomenon heavily reliant on interactions among lipid molecules and their surrounding environment. As a result, the phase transition can be influenced by factors such as pH, ionic strength, and the presence of foreign molecules, rendering it sensitive to external influences [27].

Thermal analysis through DSC thermograms, spanning temperatures from 15 ºC to 60 ºC, provides valuable information into the thermal traits of DPPG membranes and the alterations induced by MFX in the DPPG structure. Figure 2 exhibits DSC thermograms of extruded (100 nm) DPPG dispersions under low (Fig. 2 left column) and high ionic strength conditions (Fig. 2 right column). The investigations include conditions in the absence of MFX (Fig. 2a, b) and in the presence of 10 mol% MFX (Fig. 2c, d) and 20 mol% MFX (Fig. 2e, f).

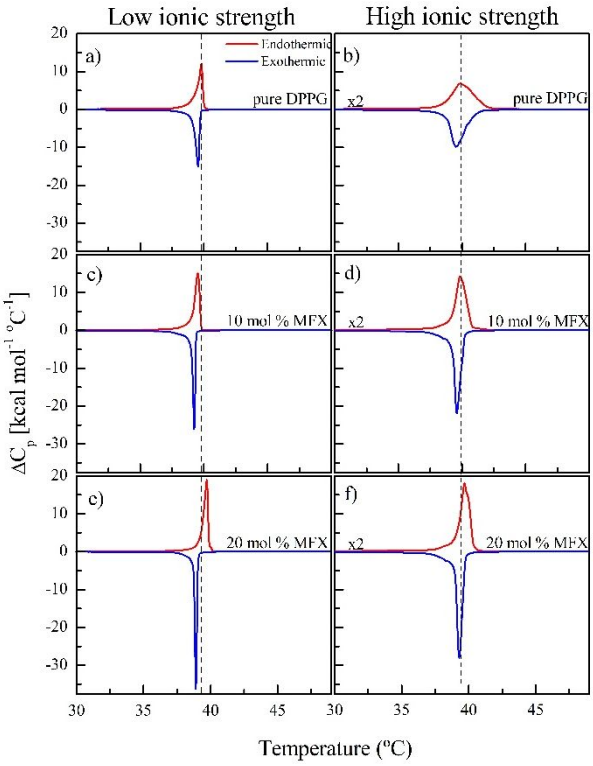

Figure 2. Typical DSC thermogram of 3 mmol L^{-1} DPPG dispersions in buffer at low (left column) and in at high ionic strength (right column) in the absence (a,b) and in the presence of increasing amounts of MFX: 10 mol% (c,d), and 20 mol% (e,f) under endothermic (red lines) and exothermic (blue lines) processes. The dotted lines are only a guide for the eyes and indicate the positions of the maximum of the thermal gel-fluid transition peak.

In both dispersions, under both low (Fig. 2a) and high ionic conditions (Fig. 2b), the DSC thermograms consistently displayed thermal peaks centered at identical positions (T_m), as indicated by overlapping standard deviation in table 1. Moreover, consistent with previous findings [17,18], DPPG dispersions demonstrate a notably reversible thermal profile (Fig. 2a and 2b). Remarkably, DPPG dispersions (Fig. 2a) under conditions of low ionic strength exhibit a more cooperative excess heat peak compared to the peak observed in DPPG dispersions under high ionic strength condition (Figure 2b), as observed before [17]. This cooperativity is evident in the smaller width at half maximum ($\Delta T_{1/2}$), as detailed in Table 1.

When considering the impact of the antibiotic on DPPG's thermotropic behavior under both low and high ionic conditions, several noteworthy observations can be made. Focusing on low ionic conditions (Fig. 2, left column), the presence of 10 mol% MFX (Fig. 2c) and 20 mol% MFX (Fig. 2e) results in a narrower transition of the gel-fluid peak compared to the transition observed in pure DPPG dispersions, particularly within the realm of exothermic processes (as indicated in Table 1). It is important to highlight that for endothermic processes, the thermal peaks with and without MFX are centered at the same temperature within standard deviation, as denoted by the dotted line in the left column of Figure 2.

Differential scanning calorimetry (DSC) thermograms of DPPG in the presence of levofloxacin (LVX), a second-generation fluoroquinolone, indicate that LVX induces the formation of antibiotic-rich and antibiotic-poor regions within DPPG membranes [17]. Interestingly, in the presence of moxifloxacin (MFX), the DPPG thermograms do not suggest the formation of such domains, as only a single thermal transition peak is observed. This behavior contrasts with that of LVX, which produces two distinct thermal transition peaks indicative of domain formation. These results suggest that MFX diffuses more uniformly into DPPG membranes than LVX, rather than remaining segregated in specific membrane regions.

$[NaCl]$ mmol L^{-1}	$mol\%$ $[MFX$	$T_m(^{o}C)$ Endothermic	$T_m(^{o}C)$ Exothermic	$\Delta H\ (kcal\ mol^{-1})$ Endothermic	$\Delta H\ (kcal\ mol^{-1})$ Exothermic	$\Delta T_{1/2}(^{o}C)$ Endotérmico	$\Delta T_{1/2}(^{o}C)$ Exothermic
3	0	39.8 ± 0.2	39.5 ± 0.1	8.8 ± 0.3	-8.4 ± 0.3	0.57±0.09	0.44±0.06
150	0	39.8 ± 0.3	39.5 ± 0.1	9.8 ± 0.9	-9.5 ± 0.8	1.5 ± 0.5	1.3 ± 0.1
3	10	39.5 ± 0.4	38.8 ± 0.5	10.3 ± 0.1	-9.65 ± 0.05	0.42 ± 0.03	0.23 ± 0.01
150	10	39.8 ± 0.4	39.6 ± 0.1	10.0 ± 0.4	-9.2 ± 0.3	0.92 ± 0.04	0.50 ± 0.07
3	20	39.70 ± 0.06	38.88 ± 0.04	9.9 ± 0.2	-8.9 ±0.2	0.33 ± 0.02	0.16 ± 0.01
150	20	39.8 ± 0.1	39.32 ± 0.04	10.9 ± 0.7	-9.3 ± 0.3	0.83 ± 0.07	0.435 ± 0.005

Table 1 summarizes the thermodynamic parameters determined through DSC thermograms

The authors [5] investigated the structural changes induced by high concentrations of MFX in extruded lipid dispersions composed of pure 1,2-dipalmitoyl-sn-glycero-3-phosphocholine (DPPC) and DPPC:cardiolipin (CL) mixtures (8:2 molar ratio), employing a lipid-to-antibiotic molar ratio close to 1:1.They demonstrated that MFX causes pronounced changes in the thermotropic behavior of zwitterionic DPPC dispersions, including the splitting of the main phase transition peak into two distinct events: one at a lower temperature (T = 33 °C) and another coinciding with the main transition of pure DPPC (≈41 °C) with a marked decrease in the intensity of the original DPPC transition peak was also observed. Interestingly, after one day of storage, the DSC thermogram of the MFX–DPPC system closely resembled that of pure DPPC, suggesting low affinity of MFX for zwitterionic membranes and progressive migration of the drug from the bilayer to the aqueous phase. In contrast, anionic dispersions composed of DPPC:CL exhibited a broad gel-to-fluid transition band centered around 30 °C. The presence of MFX caused a shift of this transition to slightly higher temperatures (by ~3 °C) and resulted in a pronounced narrowing of the thermal peak. Similar behavior was observed in our study for DPPG dispersions interacting with MFX (Fig. 2), suggesting that MFX interacts primarily at the level of the polar headgroups, promoting

closer packing of the acyl chains and enhancing the cooperativity of the thermal transition. Notably, unlike the reversible behavior observed in the MFX–DPPC system, the thermogram of the DPPC:CL–MFX system remained essentially unchanged after 24 hours of storage, reinforcing the notion that MFX exhibits greater affinity for anionic membranes [5].

3.1.2 Electron spin resonance (ESR) with spin probes

Spin label spectroscopy is widely used technique to monitor the structure/dynamic of lipid bilayers, see for example [14] This technique is very accurate to probe a lipid packing in the nano vicinity of the paramagnetic probe, moreover the ESR spectra may provide information about the polarity of the vicinity of the paramagnetic probe [14,15]. In this work, we determined the rigidity/order and the changes in the polarity at different depths of the ionic bilayers: at the levels of the 5th and the 16th carbon atoms of the lipid acyl chains, monitoring the region close to the polar headgroups, and the inner core of the bilayer, respectively. As exogenous molecules may interact differently with gel and fluid membranes, we investigated through spin label spectroscopy the structural changes induced by MFX on the anionic bilayers at temperatures ranging from 10 ºC to 60 ºC, hence analyzing the gel and fluid phases of the dipalmitoyl bilayers, see Fig. 2.

Figure 3 displays the ESR spectra of the paramagnetic probes 5-PCSL (Fig. 3a,c) and 16-PSCL (Fig. 3b,d) incorporated into gel DPPG liposomes under low ionic strength conditions (Fig. 3a,b) and high ionic strength conditions (Fig. 3c,d). Figure 3 shows spin probes spectra in the absence (black lines) and the presence of increasing amounts of MFX, 10 mol% (red lines), and 20 mol% (blue lines).

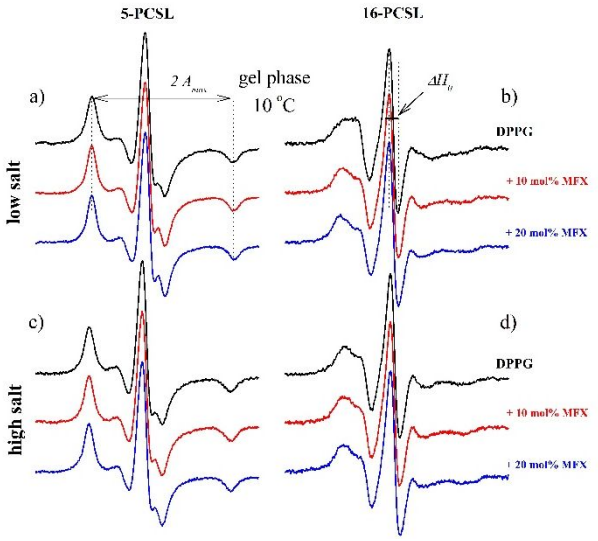

Figure 3. Typical ESR spectra of 5-PCSL (a,c) and 16-PCSL (b,d) incorporated into dispersions of gel (10 ºC) DPPG vesicles in buffer at low (a,b) and high (c,d) ionic strength. The ESR spectra were obtained in the absence of MFX (black lines), in the presence of 10 mol% (red lines) and 20 mol% MFX (blue lines). The maximum hyperfine splitting ($2\,A_{max}$) and the central line width (ΔH_0) are indicated. Total spectral width is 100 Gauss.

As discussed before [15], empirical parameters measured directly from the ESR spectra provide information of the environment of the probe. For gel membranes, the maximum outer hyperfine splitting (*2 Amax*, see Fig. 3a,c) gives information about probe's mobility. As higher *2 Amax* values, higher are the restriction of the probe's mobility (Rozenfeld et al. 2017). Fig. 4 displays the plot of *2 Amax* measured directly from 5-PCSL spectra for low (Fig. 4a) and high (Fig. 4b) ionic strength conditions as a function of temperature. DPPG dispersion at high ionic strength (Fig. 4b) yields higher *2 Amax* values than those observed for DPPG dispersions at low ionic strength (Fig. 4a). This effect is likely due to the solvation layer of counter ions that shield the anionic polar head of PG groups, thereby hindering the interaction between the acyl chain and increasing lipid packing. As expected, the increase in

temperature induced relative fluidity, evidenced by the decrease in *2 Amax* values with rising temperature, Fig. 4.

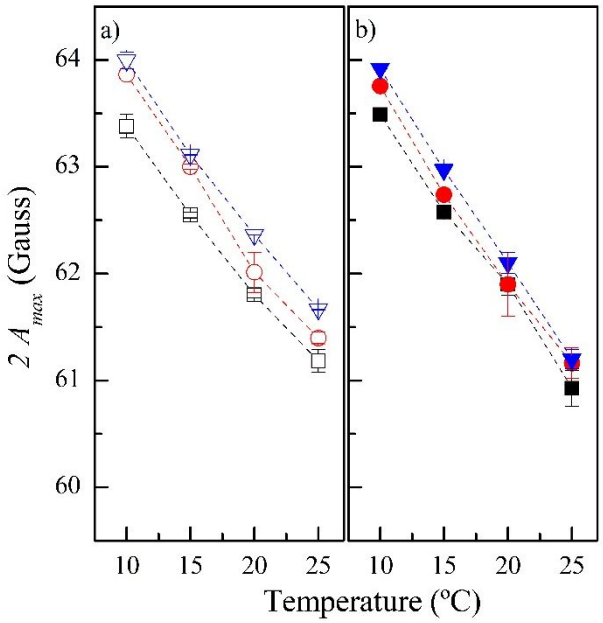

Figure 4. Temperature dependence of the outer hyperfine splitting (*2* A_{max}) measured on the ESR spectrum of 5-PSCL embedded into 3 mmol L^{-1} dispersions of gel DPPG liposomes in buffer at low (a) and high (b) ionic strength. The data were obtained in the absence of MFX (black squares), in the presence of 10 mol% MFX (red circles), and 20 mol% MFX (down blue triangles). Error bar indicates standard deviation of at least three experiments with different samples. If not shown, the deviation was found to be smaller than the symbol.

Interestingly, increasing concentrations of MFX led to an enhancement of the *2 Amax* values for DPPG dispersions under low and high ionic strength conditions (Fig. 4), suggesting that the antibiotic promotes tighter lipid packing in gel-phase DPPG vesicles at the depth of the 5th carbon.

The inner core of the DPPG vesicles were monitor by the probe 16-PCSL. For gel vesicles, the paramenter ΔH_0 (Fig. 3b), is effective in providing informations about the motion of the 16-PCSL probe, as higher ΔH_0 values, more are the restriction of the probe's moviment. Fig. 5 dispicts ΔH_0 as a function of the temperature for DPPG dispersion at low (Fig. 5a) and at high (Fig. 5b) ionic strenght conditions at absence black squares and at the presence of 10 mol% (red circles) and 20 mol% MFX (blue triangles).

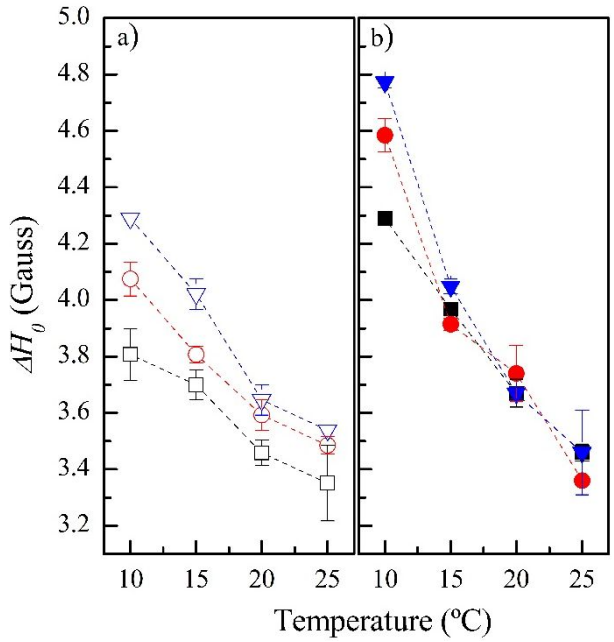

Figure 5. Temperature dependence of the central field line width (ΔH_0) measured on the ESR spectrum of 0.3 mol% of 16-PCSL embedded into 3 mmol L^{-1} dispersions of gel DPPG liposomes in buffer at low (a) and at high (b) ionic strength in the absence of MFX (black squares), in the presence of 10 mol% MFX (red circles), and 20 mol% MFX (blue down triangles). Error bar indicates standard deviation of at least three experiments with different samples. If not shown, the error bars were found to be smaller than the symbol or equal to zero.

As expected, gel-phase DPPG dispersions under low ionic strength conditions (Fig. 5a) exhibit lower ΔH_0 values compared to those observed at high ionic strength (Fig. 5b). This result likely reflects a looser lipid packing in the membrane core, attributed to reduced

shielding of the anionic headgroups under low ionic strength, which favors electrostatic repulsion between phosphatidylglycerol moieties. In contrast, at high ionic strength, the increased screening of the negative charges leads to diminished repulsion and, consequently, tighter membrane packing. The presence of 10 and 20 mol% MFX led to an increase in ΔH_0, consistent with a more restricted motion of the 16-PCSL probe. This result indicates that the antibiotic promotes tighter lipid packing near the bilayer center in DPPG dispersions under low ionic strength (Fig. 5a).

Figure 6 shows the ESR spectra of 5-PCSL (Fig. 6a,c) and 16-PCSL (Fig. 6b,d) incorporated into 3 mmol L^{-1} fluid-phase DPPG dispersions under low (Fig. 6a,b) and high ionic strength conditions (Fig. 6c,d). In all conditions, the spectra exhibit a single component, indicating that each spin label experiences a homogeneous environment within the bilayer, with no evidence of distinct populations or domains, either in the absence or in the presence of 10 and 20 mol% MFX.

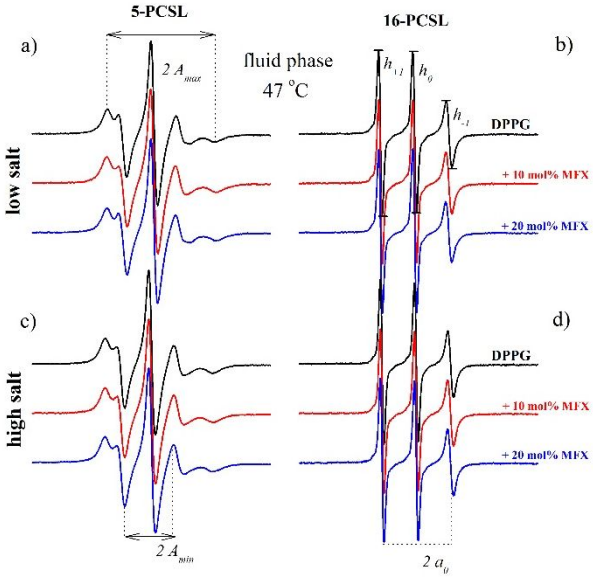

Figure 6. Typical ESR spectra of 5-PCSL (left column) and 16-PCSL (right column) incorporated into dispersions of fluid (47 ºC) DPPG liposomes in buffer at low (top panel) and high (low panel) ionic strength. The ESR spectra were obtained in the absence of MFX

(black lines), in the presence of 10 mol% (red lines) and 20 mol% MFX (blue lines). The maximum and minimum hyperfine splitting (*2 A_{max}* and *2 A_{min}*, respectively), the amplitudes of the low (h_{+1}), central (h_0) and high (h_{-1}) fields and the isotropic hyperfine splitting (a_0) are indicated. Total spectral width is 100 Gauss.

To evaluate the effects of MFX on fluid-phase DPPG membranes, we determined the effective order parameter, S_{eff} (Eq. 3), which provides information about the lipid ordering and mobility specifically at the depth corresponding to the 5th carbon atom of the acyl chain. An S_{eff} value of 1 indicates that all spin labels are perfectly aligned parallel to the bilayer normal, reflecting a highly ordered environment at this position. Conversely, S_{eff} values near zero signify rapid, isotropic, and unrestricted probe motion, characteristic of a loosely packed membrane region at the 5th carbon level, see Ref. [18] and references therein. As expected, the DPPG dispersion under low ionic strength conditions displays lower S_{eff} values (Fig. 7a) compared to DPPG under high ionic strength (Fig. 7b), reflecting reduced shielding of the anionic headgroups and consequently increased electrostatic repulsion, which leads to a less tightly packed membrane. The presence of MFX under both low and high ionic strength conditions enhanced S_{eff} values, indicating that the antibiotic promotes membrane organization at the level of the 5th carbon. LVX was also found to organize DPPG membranes at the 5th carbon [17]. Similarly, MFX has been reported to promote lipid packing near the interfacial region between the polar headgroups and the acyl chains in fluid-phase vesicles composed of DMPG under high ionic strength conditions ([NaCl]=100 mmol L^{-1}), as demonstrated by changes in bilayer organization monitored using 5-doxyl-stearic acid as a spin probe [6].

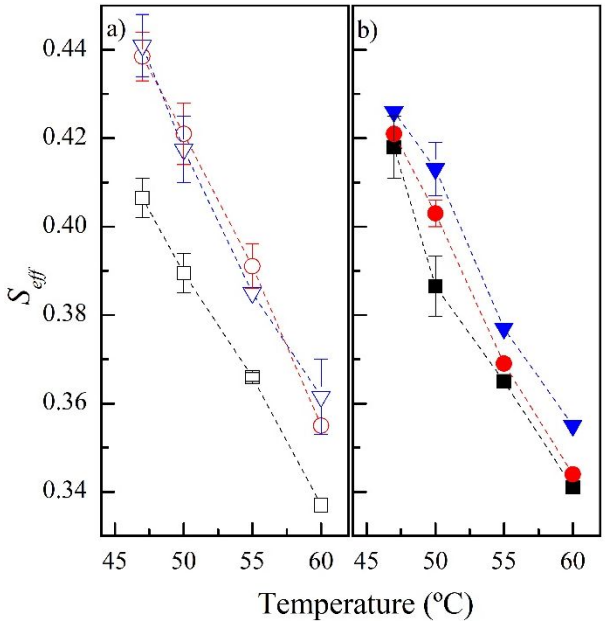

Figure 7. Temperature dependence of the effective order parameter (S_{eff}), calculated from the ESR spectra of 5-PCSL incorporated into 3 mmol L^{-1} fluid DPPG liposomes under low (a) and high (b) ionic strength conditions. Data are shown for liposomes in the absence of MFX (black squares), and in the presence of 10 mol% MFX (red circles) and 20 mol% MFX (blue downward triangles). Open and solid symbols represent samples under low and high ionic strength conditions, respectively. Error bars correspond to the standard deviation from at least three independent experiments; when not visible, they are smaller than the symbol size.

In fluid-phase bilayers, the 16-PCSL spin label typically exhibits highly dynamic motion, enabling the direct determination of the amplitudes of its three hyperfine lines (m_I = +1, 0, −1) from the ESR spectra (Fig. 8). The ratio of the high and central field lines amplitude (h_{-1}/h_0, see Fig. 6b) serves as an empirical indicator of bilayer packing: as molecular motion becomes more rapid and disordered, this ratio approaches unity [15].

Figure 8 shows the ratio h_{-1}/h_0 as a function of temperature for fluid DPPG dispersions under low (Fig. 8a) and high (Fig. 8b) ionic strength conditions. As expected, the h_{-1}/h_0 values for pure DPPG at low salt concentration are higher than those observed at high salt concentration. This difference once again reflects the shielding effect of the increased concentration of counterions under high ionic strength, which screens the polar headgroups

and promotes stronger tail-to-tail interactions, resulting in a more tightly packed bilayer region. Concerning the experiment conducted under low ionic strength conditions (Fig. 8a), the addition of 10 and 20 mol% moxifloxacin (MFX) leads to a noticeable decrease in the h_{-1}/h_0 ratio, indicating that the antibiotic promotes tighter lipid packing within the hydrophobic core of the DPPG bilayer. In contrast, under high ionic strength conditions (Fig. 8b), MFX induces only marginal changes; taking into account the associated error bars, these variations suggest that MFX does not significantly impact lipid packing in the DPPG bilayer core. Consistently, investigating the interaction of MFX with anionic DMPG dispersions at elevated salt concentrations, the authors [6] also reported no evidence of increased packing in the hydrophobic core of DMPG bilayers, as assessed using 16-doxyl stearic acid used as a spin probe.

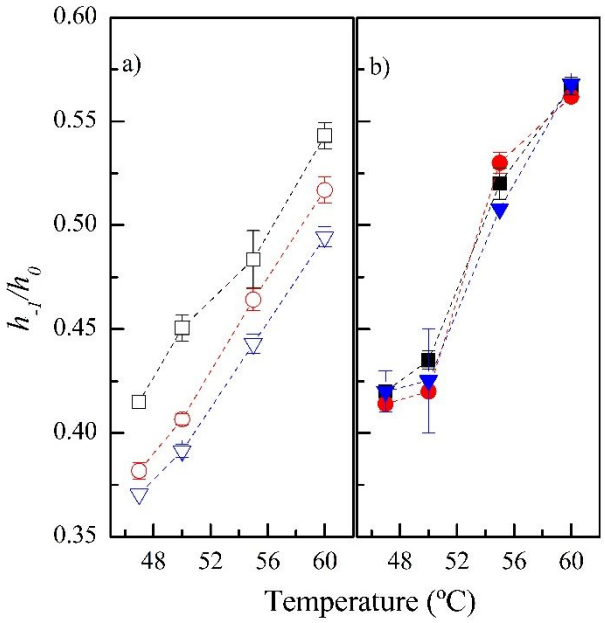

Fig. 8. Temperature dependence of the ratio of the low and central field line amplitudes, h_{-1}/h_0, measured on the ESR spectrum of 0.3 mol% of 16-PCSL embedded into 3 mmol L^{-1} dispersions of DPPG liposomes in buffer at low (a) and high (b) ionic strength. The data were obtained in the absence of MFX (black squares), and in the presence of 10 mol% MFX (red circles), and 20 mol% MFX (blue down triangles) Error bar indicates standard deviation of

at least three experiments with different samples. If not shown, the error bars were found to be smaller than the symbol or equal to zero.

The isotropic hyperfine splitting constant (a_0) provides valuable information about the local polarity of the nanoregion of the spin probe, in the present case, the membrane core. Higher a_0 values are associated with increased polarity, resulting from water penetration into this otherwise hydrophobic region [15]. Thus, variations in a_0 may reflect changes in membrane structure resulting from lipid-molecule interactions, which can affect the hydration of the lipid bilayer. Figure 9 shows a_0 values, measured directly from the 16-PCSL spectra, as a function of temperature under low (Fig. 9a) and high (Fig. 9b) ionic strength conditions, in the absence and presence of increasing MFX concentrations. The a_0 values for pure DPPG dispersions are comparable under both conditions. Upon MFX addition, a_0 values decrease across all temperatures and ionic strengths (Fig. 9a,b), indicating reduced local polarity and dehydration of the bilayer core induced by the antibiotic.

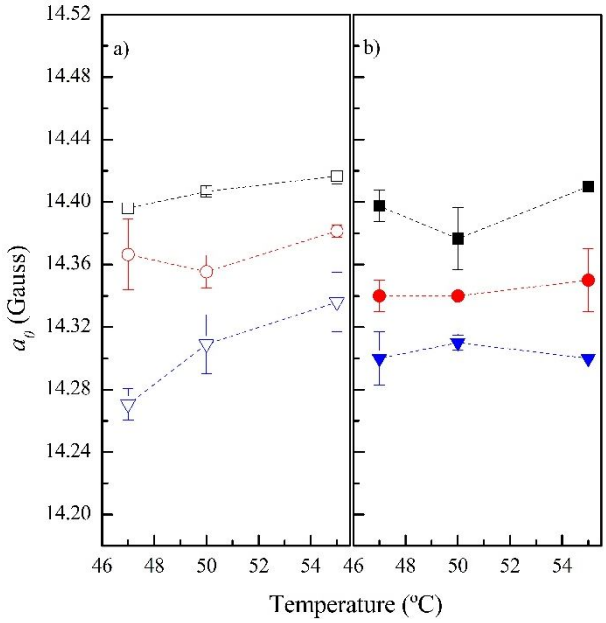

Figure 9. Temperature dependence of the isotropic hyperfine splitting (a_0) measured on ESR spectra of 0.3 mol% of 16-PCSL incorporated into 3 mmol L^{-1} dispersions of fluid (47 ºC) DPPG liposomes in buffer at low (a) and high (b) ionic strength. The data were obtained in the absence of MFX (black squares), in the presence of 10 mol % MFX (red circles), and 20 mol% MFX (blue down triangles). Error bar indicates standard deviation of at least three experiments with different samples. If not shown, the error bars were found to be smaller than the symbol or equal to zero.

3.2. Intrinsic Fluorescence Emission of MFX: Modifications Induced by Anionic Membranes

As with most fluoroquinolones (FQs), MFX is naturally fluorescent. FQ fluorescence emission is highly sensitive to the fluorophore structure and its surrounding environment [12,28,29]. Hence, we exploited MFX fluorescence to investigate its interactions with DPPG vesicles at low (Fig. 10a,c) and high ionic strength (Fig. 10b,d), obtaining information about the antibiotic's structure. At physiological pH (7.4), MFX displays a maximum emission at 466 nm (Fig. 10), in agreement with previous reports. [5,30,31]. The increase in gel (Fig. 10a) and fluid (Fig. 10c) DPPG liposome concentration under low ionic strength conditions gradually induces a significant fluorescence redshift, as shown in Figs. 10a,c and 11a. In contrast, the presence of either gel or fluid liposomes under high ionic strength conditions causes only a minor redshift of MFX emisson spectra, see Fig. 10b,c and Fig.11b.

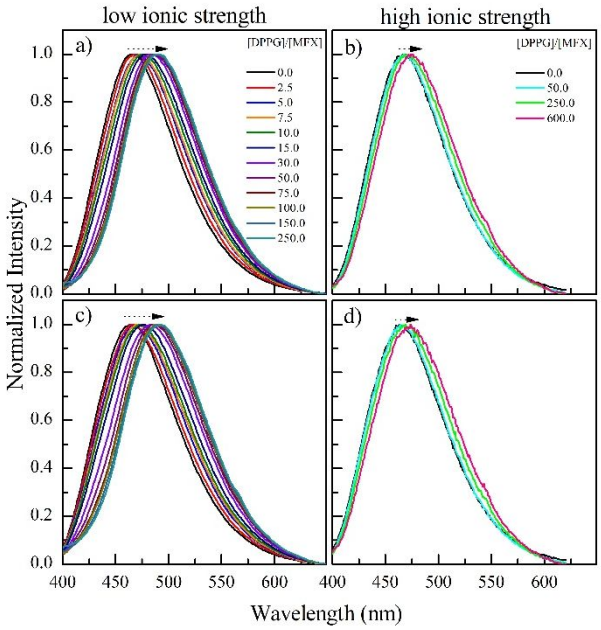

Figure 10. Emission spectra of MFX (8 μmol L^{-1}) in buffer at low (a,c) and high (b,d) ionic strength in the absence and in the presence of increasing amounts of DPPG vesicles. Excitation light beam at 345 nm.

Fluorophores typically exhibit a relative blue shift in their fluorescence spectra upon binding to lipid bilayers, reflecting the membrane's dehydrated environment and the consequent reduction in dipolar relaxation rate [32]. In our case (Figs. 10 and 11), as observed for many FQs binding to anionic structures [12,17,33], a relative red-shift occurs, likely due to the lower local pH around the anionic amphiphilic aggregate, in agreement with the Gouy–Chapman model [34]. Note that the emission of MFX under acidic conditions (low pH) occurs at longer wavelengths than that observed at physiological pH 7.4, see **Fig. SM2.** Therefore, the observed red shift in fluorescence arises from the combined effects of the transition from the zwitterionic to the cationic form of MFX and the concomitant decrease in polarity in the vicinity of the vesicle surface [12].

To further support this interpretation, plotting the fluorescence intensity at 460 nm as a function of buffer pH (Fig. **SM2**) yielded two apparent pKa values (pKa_1 = 5.8 ± 0.1 and pKa_2 = 9.91 ± 0.05), corresponding to the cationic–zwitterionic and zwitterionic–anionic equilibria of MFX, respectively. These values are close to those reported in the literature [35].

It is worth noting that the red-shift observed for the interaction with DPPG dispersions at low ionic strength is about 27 nm (Fig. 11a), compared to only 8 nm under high ionic strength conditions (Fig. 11b). This is likely due to the reduction of the surface potential of PG vesicles under high salt conditions [36] strongly indicating that the interaction between MFX and DPPG lipids is highly dependent on electrostatic interactions. Moreover, it is very interesting that the observed red-shift is the same considering the error bars for gel (25 ºC) or fluid (50 ºC) vesicles either under low and high salt concentration. Assuming a temperature-independent surface potential and applying the Gouy–Chapman model (Eq. 5), for a surface potential ranging from –100 mV to –10 mV, we calculated that the pH ratio around the PG vesicles between 25 °C and 50 °C is very close to unity, indicating that the surface pH around the vesicles remains nearly unchanged when the temperature increases from 25 °C to 50 °C.

***Eq*. 5**

$$[H_3O^+]_{surf} = [H_3O^+]_{bulk} e^{\left(-q\psi/k_BT\right)}$$

$$pH_{surf} = pH_{bulk} + 0.434\ \frac{q\psi}{k_BT}$$

In these expressions $[H_3O^+]_{surf}$ and $[H_3O^+]_{bulk}$ denote the hydronium concentrations at the vesicle surface and in the bulk phase, respectively; pH_{surf} and pH_{bulk}

refer to the corresponding pH values; is the elementary charge; $\psi$is the vesicle surface potential; $k_B$is the Boltzmann constant; and $T$is the absolute temperature[12].

This is may account for the observed red shift and suggests that MFX has comparable affinity for both gel-phase and fluid-phase PG membranes. Taking into account that the antibiotic, once zwitterionic, becomes cationic, it is highly probable that MFX is located close to the vesicle surface.

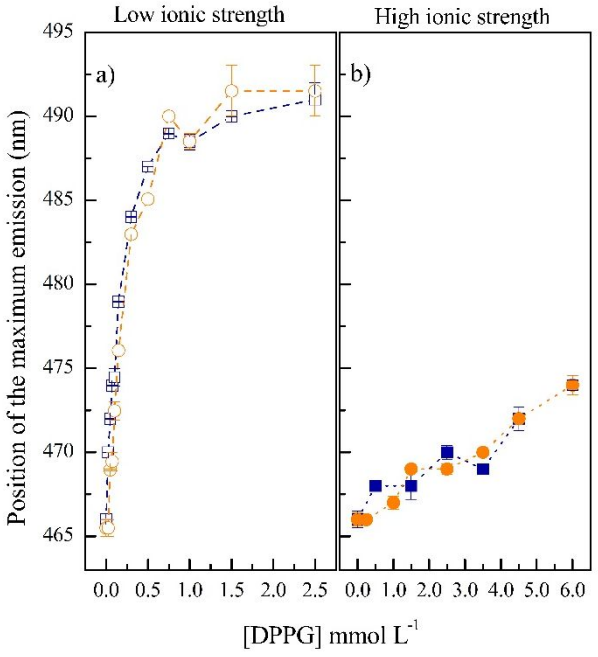

Figure 11. Position of the maximum emission of MFX in buffer at low (a) and high (b) ionic strength as a function of the concentration of gel (25 ºC, blue squares) and fluid (50 ºC, orange circles) DPPG vesicles.

Fluorescence spectra can be significantly affected by light scattering, often caused by liposomes. Although the presented spectra were corrected by using Eq. 2, the use of a complementary technique was considered important. Consequently, time-resolved fluorescence was employed, a method minimally influenced by light scattering [21,32], allowing the determination of excited-state lifetimes through analysis of fluorescence decay curves.

Figure 12 shows the fluorescence decay curves of MFX in the absence and in the presence of DPPG dispersions under low (Figs. 12a,c) and high (Figs. 12b,d) ionic strength, with the liposomes in the gel phase (25 °C, Figs. 12a,b) and fluid phase (50 °C, Figs. 12c,d).

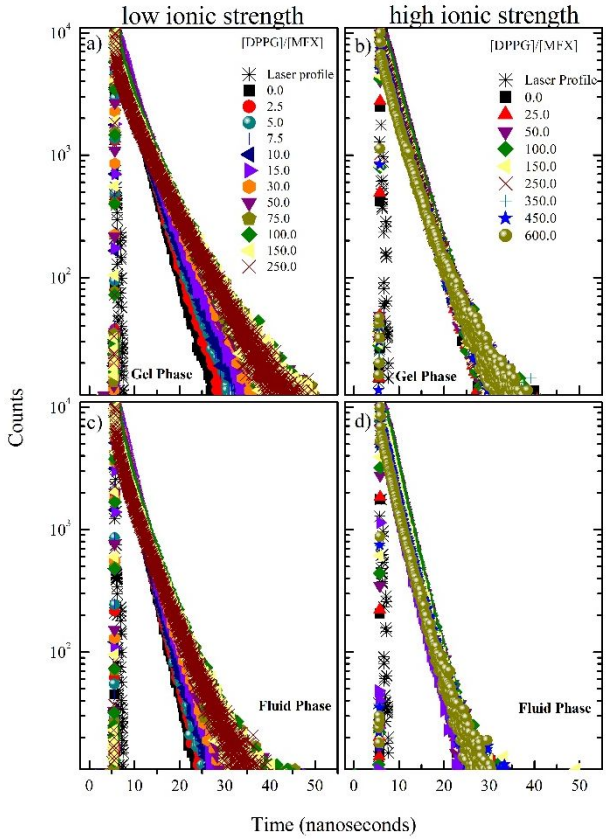

Figure 12. Typical fluorescence decay curves of MFX in buffer at low (a,c) and high (b,d) ionic strength in the presence of increasing concentrations of gel vesicles (25ºC) of DPPG (a,b) and fluid vesicles (50 ºC) of DPPG. Excitation light beam at 284 nm and emission at 466 nm.

MFX fluorescence decay curves, both in the absence and in the presence of liposomes, were well fitted by a biexponential model, according to statistical criteria, yielding two fluorescence lifetimes, a short lifetime (τ_1) and a long lifetime (τ_2). At 25 ºC, τ_1 = (2.65 ± 0.08) ns and τ_2 = (3.5 ± 0.1) ns were found. As expected, increasing the temperature to 50

ºC led to a reduction in the fluorescence lifetimes due to the enhancement of non-radiative decay rates, with the observed values being τ_1 = (1.4 ± 0.2) ns and τ_2 = (2.80 ± 0.04) ns.

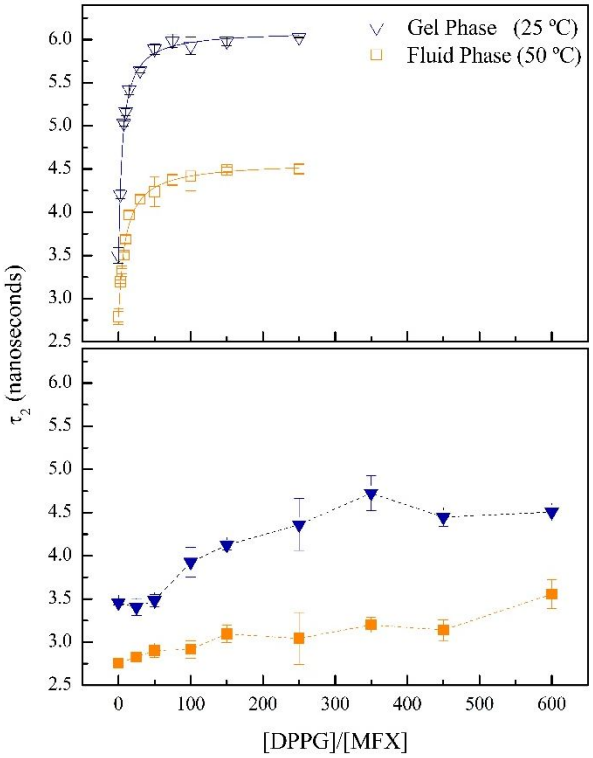

Figure 13. Longer fluorescence lifetime of MFX (τ_2) in buffer at low (a) and high (b) ionic strength as a function of gel (25 ºC) vesicles (blue squares) and fluid (50 ºC) vesicles (orange circles) of DPPG. The continuous lines consist in the data fitting by using eq. X. The dotted lines are only guide for the eyes.

Fig. 13 shows the long lifetime of MFX (τ_2) as a function of DPPG dispersions in the gel phase (25 ºC; blue downward triangles) and fluid phase (50 ºC; orange squares) under low ionic strength (Fig. 13a) and high ionic strength (Fig. 13b) conditions. Under low ionic strength, the long lifetime of MFX increased monotonically in the presence of DPPG dispersions, allowing the data to be fitted using Eq. 4 and enabling the determination of distinct partition constants: $K_p = (2.7 \pm 0.2) \times 10^4$ for gel membranes (25 ºC) and K_p = (1.4

± 0.1) × 10^4 for fluid membranes (50 ºC). Considering that the partition constant is temperature-dependent, the values obtained suggest that MFX exhibits very similar affinity for both gel and fluid DPPG membranes. Additionally, as indicated by steady-state and time-resolved fluorescence, increasing the ionic strength reduces the affinity of the antibiotic for anionic membranes. Under high salt conditions, the lifetimes (Fig. 13b) do not reach saturation, indicating that most MFX molecules remain in the aqueous environment rather than binding to the liposomes. This strongly suggests that the interaction is highly dependent on electrostatic attraction between the antibiotic and the lipid polar headgroups.

Interestingly, MFX exhibits a partition constant (K_p) that is two orders of magnitude higher than that of LVX for DPPG membranes under very similar conditions, indicating that MFX is more lipophilic than LVX [17]. This is particularly relevant given that MFX does not depend on protein channels in the bacterial membrane to access the cytosol, unlike LVX, which requires porin-mediated uptake.

4. Conclusions

MFX significantly modulates the physicochemical properties of anionic DPPG membranes, with effects consistently observed under both gel and fluid phases. DSC traces revealed that MFX narrows the gel-to-fluid phase transition peak, indicating enhanced cooperativity of lipid packing without evidence of domain separation. ESR spectroscopy corroborated these findings, showing that MFX promotes tighter lipid organization both near the interfacial region and in the bilayer core, accompanied by a decrease polarity in the core of the anionic liposomes. Fluorescence experiments further confirmed that MFX associates strongly with DPPG membranes under low ionic strength, with partition constants on the order of 10^4, for liposomes in both configurations: in the gel and fluid phases. Whereas high

ionic strength markedly reduces this affinity, emphasizing the electrostatic nature of the interaction MFX-DPPG. Altogether, the data indicate that MFX preferentially locates at the lipid–water interface, where protonation driven by the negatively charged environment may occur, thereby altering the antibiotic's structure. Given that membrane interactions are critical to antimicrobial activity, toxicity, and drug delivery, these results provide important physicochemical insights into the behavior of MFX in lipid environments and may guide the rational design of lipid-based carriers and the optimization of fluoroquinolone antibiotics.

5.Declaration of competing interest

The authors declare that they have no known competing financial interests or personal relationships that could have appeared to influence the work reported in this paper.

6.Acknowledgments

This work was supported by FAPESP, CNPq, CAPES, and the Central Analítica of the Institute of Chemistry of University of Brasília.

7. References

(1) Pham, T. D. M.; Ziora, Z. M.; Blaskovich, M. A. T. Quinolone Antibiotics. *MedChemComm* **2019**, *10* (10), 1719–1739. https://doi.org/10.1039/C9MD00120D.

(2) Ajani, O. O.; Iyaye, K. T.; Ademosun, O. T. Recent Advances in Chemistry and Therapeutic Potential of Functionalized Quinoline Motifs – a Review. *RSC Adv.* **2022**, *12* (29), 18594–18614. https://doi.org/10.1039/D2RA02896D.

(3) Danilchanka, O.; Pavlenok, M.; Niederweis, M. Role of Porins for Uptake of Antibiotics by *Mycobacterium Smegmatis*. *Antimicrob. Agents Chemother.* **2008**, *52* (9), 3127–3134. https://doi.org/10.1128/AAC.00239-08.

(4) Leus, I. V.; Adamiak, J.; Chandar, B.; Bonifay, V.; Zhao, S.; Walker, S. S.; Squadroni, B.; Balibar, C. J.; Kinarivala, N.; Standke, L. C.; Voss, H. U.; Tan, D. S.; Rybenkov, V.

V.; Zgurskaya, H. I. Functional Diversity of Gram-Negative Permeability Barriers Reflected in Antibacterial Activities and Intracellular Accumulation of Antibiotics. *Antimicrob. Agents Chemother.* **2023**, *67* (2), e01377-22. https://doi.org/10.1128/aac.01377-22.

(5) Le-Deygen, I. M.; Skuredina, A. A.; Safronova, A. S.; Yakimov, I. D.; Kolmogorov, I. M.; Deygen, D. M.; Burova, T. V.; Grinberg, N. V.; Grinberg, V. Y.; Kudryashova, E. V. Moxifloxacin Interacts with Lipid Bilayer, Causing Dramatic Changes in Its Structure and Phase Transitions. *Chem. Phys. Lipids* **2020**, *228*, 104891. https://doi.org/10.1016/j.chemphyslip.2020.104891.

(6) Neves, P.; Leite, A.; Rangel, M.; de Castro, B.; Gameiro, P. Influence of Structural Factors on the Enhanced Activity of Moxifloxacin: A Fluorescence and EPR Spectroscopic Study. *Anal. Bioanal. Chem.* **2007**, *387* (4), 1543–1552. https://doi.org/10.1007/s00216-006-1009-x.

(7) Lee, T.-H.; Charchar, P.; Separovic, F.; Reid, G. E.; Yarovsky, I.; Aguilar, M.-I. The Intricate Link between Membrane Lipid Structure and Composition and Membrane Structural Properties in Bacterial Membranes. *Chem. Sci.* **2024**, *15* (10), 3408–3427. https://doi.org/10.1039/D3SC04523D.

(8) Mingeot-Leclercq, M.-P.; Décout, J.-L. Bacterial Lipid Membranes as Promising Targets to Fight Antimicrobial Resistance, Molecular Foundations and Illustration through the Renewal of Aminoglycoside Antibiotics and Emergence of Amphiphilic Aminoglycosides. *MedChemComm* **2016**, *7* (4), 586–611. https://doi.org/10.1039/C5MD00503E.

(9) Klein, M. E.; Rieckmann, M.; Lucas, H.; Meister, A.; Loppnow, H.; Mäder, K. Phosphatidylserine (PS) and Phosphatidylglycerol (PG) Enriched Mixed Micelles (MM): A New Nano-Drug Delivery System with Anti-Inflammatory Potential? *Eur. J. Pharm. Sci.* **2020**, *152*, 105451. https://doi.org/10.1016/j.ejps.2020.105451.

(10) Loew, C.; Riske, K. A.; Lamy, M. T.; Seelig, J. Thermal Phase Behavior of DMPG Bilayers in Aqueous Dispersions as Revealed by^{2} H- and^{31} P-NMR. *Langmuir* **2011**, *27* (16), 10041–10049. https://doi.org/10.1021/la201027p.

(11) Riske, K. A.; Barroso, R. P.; Vequi-Suplicy, C. C.; Germano, R.; Henriques, V. B.; Lamy, M. T. Lipid Bilayer Pre-Transition as the Beginning of the Melting Process. *Biochim. Biophys. Acta BBA - Biomembr.* **2009**, *1788* (5), 954–963. https://doi.org/10.1016/j.bbamem.2009.01.007.

(12) Muniz, G. S. V.; Teixeira, L. R.; Louro, S. R. W. Interaction of the Antibiotic Norfloxacin with Ionic Micelles: pH-Dependent Binding. *Eur. Biophys. J.* **2014**, *43* (10–11), 477–483. https://doi.org/10.1007/s00249-014-0978-5.

(13) McConnell, H. M.; Hubbell, W. L. Molecular Motion in Spin-Labeled Phospholipids and Membranes. *J. Am. Chem. Soc.* **1971**, *93* (2), 314–326. https://doi.org/10.1021/ja00731a005.

(14) Marsh, D. *Membrane Spectroscopy*; In: Grell, E. (Ed.) Springer Berlin Heidelberg: Berlin, Heidelberg, 1981; Vol. 31. https://doi.org/10.1007/978-3-642-81537-9.

(15) Rozenfeld, J. H. K.; Duarte, E. L.; Oliveira, T. R.; Lamy, M. T. Structural Insights on Biologically Relevant Cationic Membranes by ESR Spectroscopy. *Biophys. Rev.* **2017**, *9* (5), 633–647. https://doi.org/10.1007/s12551-017-0304-4.

(16) Vivas, C. V.; Da Cunha, A. R.; Lamy, M. T.; Duarte, E. L.; Vignoli Muniz, G. S. DODAB-ODN Lipoplex Structure Is Highly Dependent on ODN Concentration: A Multitechnique Experimental Study. *Biochem. Biophys. Rep.* **2025**, *43*, 102128. https://doi.org/10.1016/j.bbrep.2025.102128.

(17) Vignoli Muniz, G. S.; Souza, M. C.; Duarte, E. L.; Lamy, M. T. Comparing the Interaction of the Antibiotic Levofloxacin with Zwitterionic and Anionic Membranes: Calorimetry, Fluorescence, and Spin Label Studies. *Biochim. Biophys. Acta BBA - Biomembr.* **2021**, 183622. https://doi.org/10.1016/j.bbamem.2021.183622.

(18) Vignoli Muniz, G. S.; Duarte, E. L.; Lorenzón, E. N.; Cilli, E. M.; Lamy, M. T. What Different Physical Techniques Can Disclose about Disruptions on Membrane Structure Caused by the Antimicrobial Peptide Hylin A1 and a More Positively Charged Analogue. *Chem. Phys. Lipids* **2022**, *243*, 105173. https://doi.org/10.1016/j.chemphyslip.2022.105173.

(19) Mendonça, A.; Rocha, A. C.; Duarte, A. C.; Santos, E. B. H. The Inner Filter Effects and Their Correction in Fluorescence Spectra of Salt Marsh Humic Matter. *Anal. Chim. Acta* **2013**, *788*, 99–107. https://doi.org/10.1016/j.aca.2013.05.051.

(20) *Principles of Fluorescence Spectroscopy*; Lakowicz, J. R., Ed.; Springer US: Boston, MA, 2006. https://doi.org/10.1007/978-0-387-46312-4.

(21) Santos, N. C.; Prieto, M.; Castanho, M. A. R. B. Quantifying Molecular Partition into Model Systems of Biomembranes: An Emphasis on Optical Spectroscopic Methods.

Biochim. Biophys. Acta BBA - Biomembr. **2003**, *1612* (2), 123–135. https://doi.org/10.1016/S0005-2736(03)00112-3.

(22) Marsh, D. *Handbook of Lipid Bilayers*, 0 ed.; CRC Press, 2013. https://doi.org/10.1201/b11712.

(23) Matos, P. M.; Franquelim, H. G.; Castanho, M. A. R. B.; Santos, N. C. Quantitative Assessment of Peptide–Lipid Interactions. *Biochim. Biophys. Acta BBA - Biomembr.* **2010**, *1798* (11), 1999–2012. https://doi.org/10.1016/j.bbamem.2010.07.012.

(24) Heimburg, T. *Thermal Biophysics of Membranes*; Tutorials in biophysics; Wiley-VCH Verlag: Weinheim, 2007.

(25) Tamashiro, M. N.; Henriques, V. B.; Lamy, M. T. Aqueous Suspensions of Charged Spherical Colloids: Dependence of the Surface Charge on Ionic Strength, Acidity, and Colloid Concentration. *Langmuir* **2005**, *21* (24), 11005–11016. https://doi.org/10.1021/la051211q.

(26) Enoki, T. A.; Henriques, V. B.; Lamy, M. T. Light Scattering on the Structural Characterization of DMPG Vesicles along the Bilayer Anomalous Phase Transition. *Chem. Phys. Lipids* **2012**, *165* (8), 826–837. https://doi.org/10.1016/j.chemphyslip.2012.11.002.

(27) Prenner, E.; Chiu, M. Differential Scanning Calorimetry: An Invaluable Tool for a Detailed Thermodynamic Characterization of Macromolecules and Their Interactions. *J. Pharm. Bioallied Sci.* **2011**, *3* (1), 39. https://doi.org/10.4103/0975-7406.76463.

(28) Vignoli Muniz, G. S.; Incio, J. L.; Alves, O. C.; Krambrock, K.; Teixeira, L. R.; Louro, S. R. W. Fluorescence and Electron Paramagnetic Resonance Studies of Norfloxacin and N-Donor Mixed-Ligand Ternary Copper(II) Complexes: Stability and Interaction with SDS Micelles. *Spectrochim. Acta. A. Mol. Biomol. Spectrosc.* **2018**, *189*, 133–138. https://doi.org/10.1016/j.saa.2017.08.013.

(29) Albini, A.; Monti, S. Photophysics and Photochemistry of Fluoroquinolones. *Chem. Soc. Rev.* **2003**, *32* (4), 238. https://doi.org/10.1039/b209220b.

(30) Lorenzo, F.; Navaratnam, S.; Edge, R.; Allen, N. S. Primary Photophysical Properties of Moxifloxacin— A Fluoroquinolone Antibiotic. *Photochem. Photobiol.* **2008**, *84* (5), 1118–1125. https://doi.org/10.1111/j.1751-1097.2007.00269.x.

(31) Lopes, S. C.; Ribeiro, C.; Gameiro, P. A New Approach to Counteract Bacteria Resistance: A Comparative Study Between Moxifloxacin and a New Moxifloxacin Derivative in Different Model Systems of Bacterial Membrane. *Chem. Biol. Drug Des.* **2013**, *81* (2), 265–274. https://doi.org/10.1111/cbdd.12071.

(32) Valeur, B. *Molecular Fluorescence: Principles and Applications*; Wiley-VCH: Weinheim ; New York, 2002.

(33) Paul, B. K.; Ghosh, N.; Mukherjee, S. Interplay of Multiple Interaction Forces: Binding of Norfloxacin to Human Serum Albumin. *J. Phys. Chem. B* **2015**, *119* (41), 13093–13102. https://doi.org/10.1021/acs.jpcb.5b08147.

(34) Evans, D. F.; Wennerström, H. *The Colloidal Domain: Where Physics, Chemistry, Biology, and Technology Meet*, 2nd ed.; Advances in interfacial engineering series; Wiley-VCH: New York, 1999.

(35) Langlois, M.-H.; Montagut, M.; Dubost, J.-P.; Grellet, J.; Saux, M.-C. Protonation Equilibrium and Lipophilicity of Moxifloxacin. *J. Pharm. Biomed. Anal.* **2005**, *37* (2), 389–393. https://doi.org/10.1016/j.jpba.2004.10.022.

(36) Riske, K. A.; Nascimento, O. R.; Peric, M.; Bales, B. L.; Lamy-Freund, M. T. Probing DMPG Vesicle Surface with a Cationic Aqueous Soluble Spin Label. *Biochim. Biophys. Acta BBA - Biomembr.* **1999**, *1418* (1), 133–146. https://doi.org/10.1016/S0005-2736(99)00019-X.